Abridged version

KAWASAKI STEEL TECHNICAL REPORT
No.9 (March 1984)

Development of Heavy-wall 2 1/4Cr-1Mo Forgings

Kazuo Aso, Hidefumi Tani, Takuichi Imanaka, Shingo Sato, Yoshifumi Nakano, Shinji Sato

Synopsis :
Generally, a 2 1/4Cr-1Mo steel is used as material for the pressure vessels of oil refining and the like, with requirement for greater thickness, high strength, high toughness, and little embrittlement in operation. With this background, experimental manufacture has been performed of a heavy section 2 1/4Cr-1Mo forged shell ring (t=400mm). To reduce embrittlement susceptibility, a low Si-low P type steel was selected and to give strength even at midsection, high austenitizing temperatures were used. Test results showed high strength and toughness even with greater thickness, as well as little temper embrittlement, hydrogen damage and creep embrittlement.

The body can be viewed from the next page.

KAWASAKI STEEL TECHNICAL REPORT No. 9 March 1984

Development of Heavy-wall 2¼Cr-1Mo Forgings*

Kazuo ASO** Hidefumi TANI** Takuichi IMANAKA***
Shingo SATO*** Yoshifumi NAKANO*** Shinji SATO***

Generally, a 2¼Cr-1Mo steel is used as material for the pressure vessels of oil refining and the like, with requirement for greater thickness, high strength, high toughness, and little embrittlement in operation.

With this background, experimental manufacture has been performed of a heavy section 2¼Cr-1Mo forged shell ring (t = 400 mm). To reduce embrittlement susceptibility, a low Si-low P type steel was selected and to give strength even at midsection, high austenitizing temperatures were used.

Test results showed high strength and toughness even with greater thickness, as well as little temper embrittlement, hydrogen damage and creep embrittlement.

1 Introduction

In oil refinery and other industries, pressure vessels have been built increasingly larger in recent years from the standpoint of production efficiency, with noticeable changes in operating conditions such as higher temperatures and higher pressures. These pressure vessels are mainly made of 2¼Cr-1Mo steels, with a growing trend toward larger use of forgings in view of quality requirement and reliability. Thus there is an increasing demand for extra-heavy forgings of minimum embrittlement in service.

Especially, principal pressure vessels such as desulfurization towers are made of 2¼Cr-1Mo steels that are not only of minimum in-service embrittlement but also excellent in mechanical properties at elevated temperatures and anti-hydrogen attack properties.

As reported already, it is advantageous to use hollow ingots because of their excellent homogeneity and other features in producing forgings such as those for pressure vessels. In producing forgings as thick as about 400 mm, however, it is necessary to review the steelmaking process itself for obtaining high cleanliness and excellent homogeneity. Furthermore, in ensuring high strength and high toughness to 2¼Cr-1Mo extra-heavy steel forgings, a proper heat treatment is necessary to improve mechanical properties.

In manufacturing a 400 mm wall-thickness shell ring of 2¼Cr-1Mo forging, efforts were made to assure the steel of cleanliness and uniformity by using a hollow ingot processed in the BOF–RH while care was taken to secure high strength and high toughness by adopting a low-Si, low-P steel and a high temperature quenching.

Based on satisfactory results obtained from the above, this paper presents the results of the shell ring manufacture, together with the results of tests conducted to examine anti-hydrogen attack properties.

2 Chemical Composition Design and Heat Treatment Conditions for Extra-Heavy Steels

To increase the strength and toughness of 2¼Cr-1Mo steels, it is necessary to obtain a uniform bainite structure. For this purpose, the austenite grain size at quenching is also important although it is effective to add elements that improve hardenability. **Figure 1** shows the relationship between the mechanical properties and austenite grain size of the steel heat-treated in a condition similar to that of 400 mm thickness. When the austenite grain size is finer than ASTM No. 6, ferrite precipitates and strength, especially yield strength, decreases remarkably. When the austenite grain size is coarser than ASTM No. 5, toughness decreases a little as the grains coarsen. However, the degree of this deterioration in toughness is low and high strength can be ensured.

* Originally published in *Kawasaki Steel Giho*, **15** (1983) 4, pp. 249–257
** Mizushima Works
*** Research Laboratories

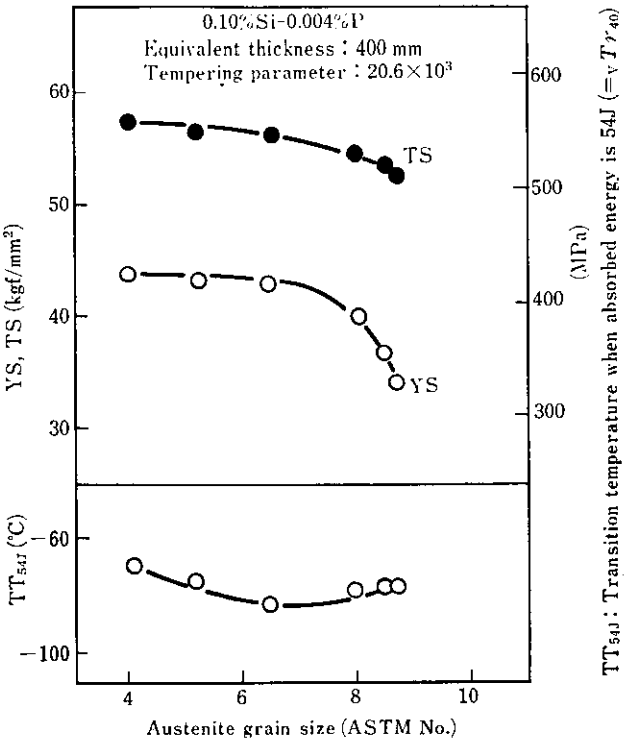

Fig. 1 Effect of austenite grain size on mechanical properties of heavy section 2¼Cr-1Mo steel

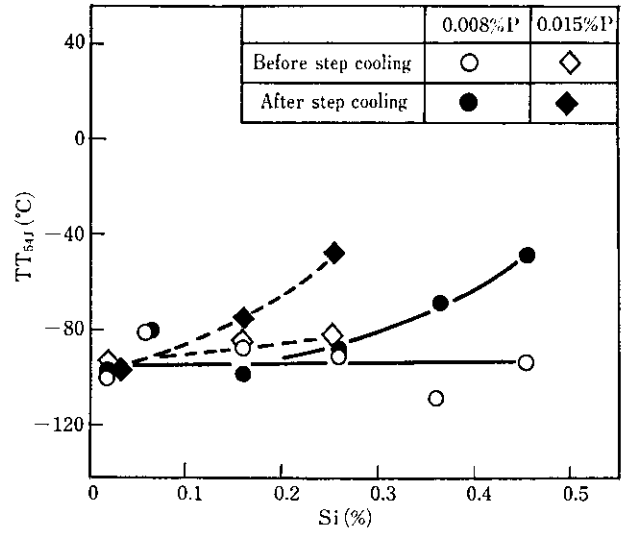

Fig. 2 Effect of silicon and phosphorus contents on temper embrittlement

Figure 2 shows the relationship[1] between the temper embrittlement susceptibility and the Si and P contents of 2¼Cr-1 Mo steels. **Figure 3** shows the relationship between the temper embrittlement susceptibility and

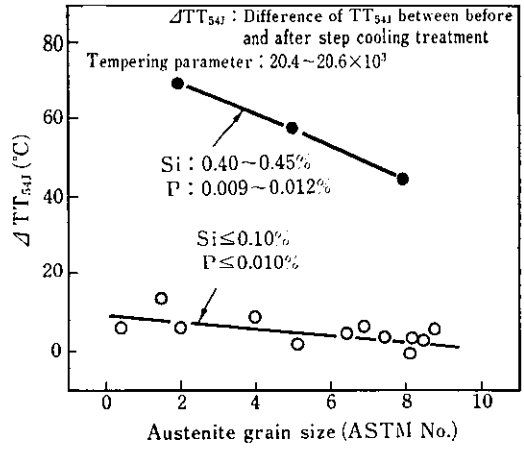

Fig. 3 Relation between temper embrittlement susceptibility and austenite grain size of 2¼Cr-1Mo steel

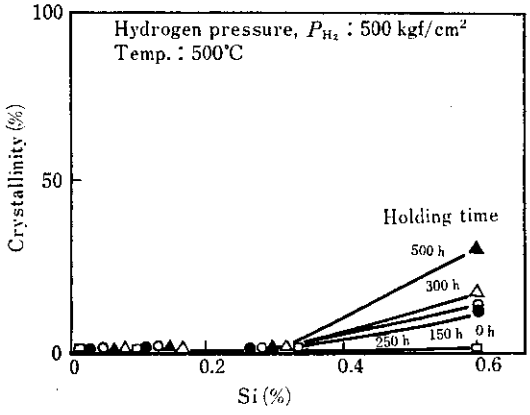

Fig. 4 Effect of Si content on crystallinity of test steel after hydrogen exposure

the austenite grain size. If Si and P are less than or equal to 0.10% and 0.010%, respectively, the amount of increase in TT_{54J} (transition temperature indicating 54J) caused by step cooling (SC) can be controlled to below 10°C even if the austenite grain size coarsens. An investigation was made into the effect of the Si content on the resistance to hydrogen attack using a 100 kg ingot obtained by a vacuum refining process. **Figure 4** shows results of this investigation. The resistance to hydrogen attack increases with decreasing Si content. Further, lowering the Si content has a favorable effect on creep characteristics[2]. From these points of view, it was decided to use a low-Si steel (Si $\leq$ 0.10%). Also, to inhibit a decrease in strength at elevated temperatures resulting from the lowered Si content, chemical composition was so designed as to aim the upper limits of C, Cr and Mo ingiven specifications, with some addition of Cu and Ni.

3 Quality Characteristics of 2¼Cr-1Mo Forging for Shell Ring

3.1 Test Materials

Figure 5 shows the manufacturing process[3] of a 2¼Cr-1Mo steel forging for shell ring. Molten pig iron was desulfurized twice in the desulfurizing process and was then dephosphorized and refined by the double-blowing method in a basic oxygen furnace. After the degassing and composition adjustment in an RH degassing unit, the molten steel was bottom-poured to cast a 200 t hollow ingot. **Photo 1** shows the appear-

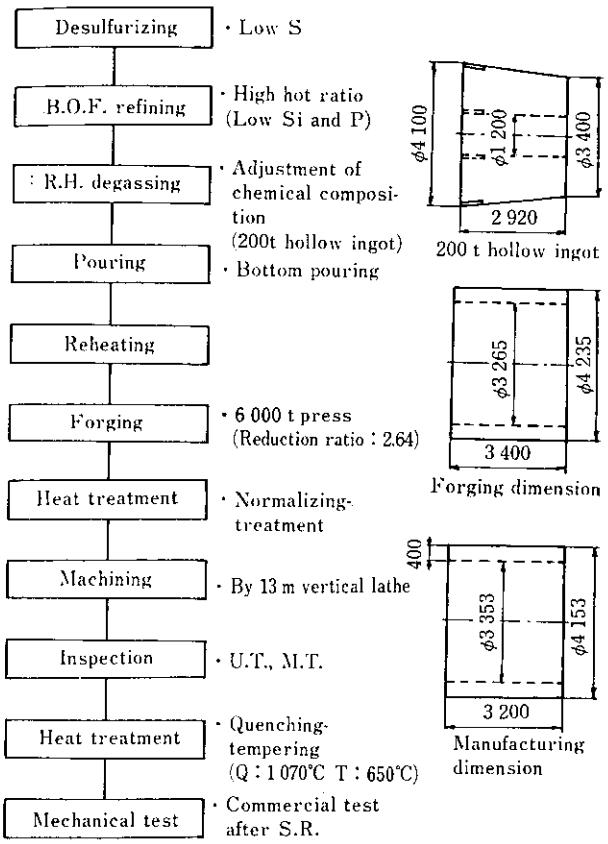

Fig. 5 Manufacturing process and its condition of heavy section shell ring

Photo 1 External view of 200 t hollow ingot

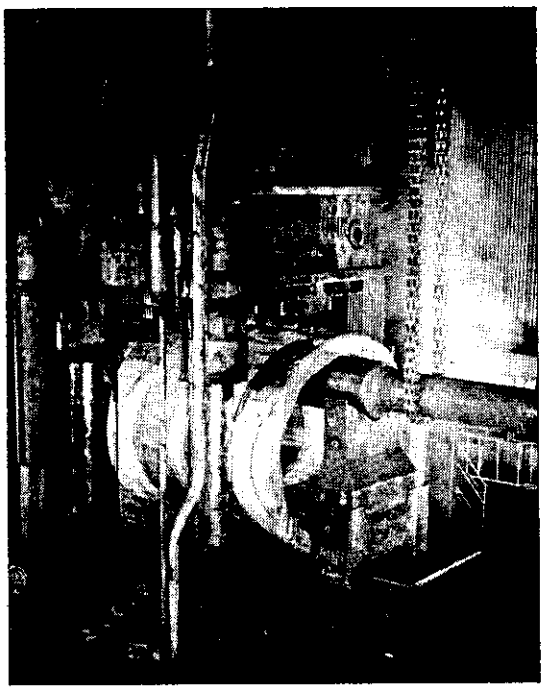

Photo 2 Forging of heavy section 2¼Cr-1Mo steel shell ring from 200 t hollow ingot

Table 1 Chemical requirements and composition of molten steel for 200 t hollow ingot (wt. %)

	C	Si	Mn	P	S	Cu	Ni	Cr	Mo	V	Al	As	Sn	Sb	B	Nb	Co
SA336 Cl. F22 Spec.	≤0.15	≤0.50	0.30 ~0.60	≤ 0.030	≤ 0.030	—	—	2.00 ~2.50	0.90 ~1.10	—	—	—	—	—	—	—	—
Aimed value	0.14 ~0.15	0.05 ~0.10	0.50 ~0.55	≤ 0.008	≤ 0.003	0.10 ~0.20	0.10 ~0.20	2.35 ~2.45	1.00 ~1.10	≤ 0.030	0.010 ~ 0.025	≤ 0.004	≤ 0.002	≤ 0.000 5	≤ 0.000 3	≤ 0.005	≤ 0.005
Heat analysis	0.14	0.10	0.53	0.004	0.003	0.16	0.16	2.45	1.03	0.011	0.020	0.002	≤ 0.001	0.000 5	0.000 1	0.001	0.005

ance of the 200 t hollow ingot. **Table 1** gives the ladle analysis of the molten steel. The ingot was forged into a forging 4 235 mm in outside diameter, 3 265 mm in inside diameter and 3 400 mm in length using a 6 000 t free forging press. **Photo 2** shows the ingot being forged. Forging was followed by preliminary heat treatment, machining (to 4 153 mm in outside diameter, 3 353 mm in inside diameter and 3 200 mm in length) and heat treatment (water quenched from 1 070°C and tempering at 650°C). The shell ring thus produced was tested.

3.2 Test Method

Figure 6 shows sampling positions of test blocks. The test blocks ① and ⑥ were used to investigate homogeneity and cleanliness by testing the chemical composition, microstructure, etc. The test blocks ② and ⑤ were used to investigate basic properties such as mechanical properties including tensile properties at room temperature (ASTM A370, see Fig. 6), tensile properties at elevated temperatures (ASTM E8), Charpy impact value (ASTM A370, see Fig. 11, Type A) and drop-weight test value (ASTM E208 P-3). Furthermore, the static three-point bending test (ASTM E399), CT test (ASTM E399) and compact test (ASTM E24, Type MRL recommended by the Committee) were conducted as fracture toughness tests to investigate, respectively, critical COD (δ), static fracture toughness (K_{Ic}) and crack arrest toughness (K_{Ia}).

Moreover, the low-cycle fatigue test was conducted on the test block ② at room temperature and an elevated temperature (482°C) to investigate fatigue properties. The test conditions are as follows:

(1) Specimen: Specimen with parallel area and sand-glass-type specimen
(2) Control method: Axial strain control (partly, diametrical strain control)
(3) Wave shape: Triangle
(4) Strain rate: $2 \times 10^{-3} s^{-1}$
(5) Heating method: High-frequency induction heating
(6) Indication of life: Number of cycles observed when the tension side load decreases by 25% from the level in a stable condition

The tests were conducted in the as-quench-tempered condition, after postweld heat treatment, and after SC, to confirm various properties of the materials.

3.3 Test Results

3.3.1 Homogeneity and cleanliness

Figure 7 shows results of a check analysis. The segregation in both the top and the bottom is very slight and the chemical composition is uniform in the whole section of the wall thickness of 400 mm. **Photo 3** shows an example of typical microstructure. Bainite is uniform from the surfaces to the middle of the thickness. **Table 2** shows results of the cleanliness test. The cleanlines index dT (60 × 400) ranges from 0.025 to 0.037%. The number of inclusions is small in spite of the use of a large ingot.

It seems that this good homogeneity and cleanliness are due largely to the use of a hollow ingot and the adoption of the bottom pouring process.

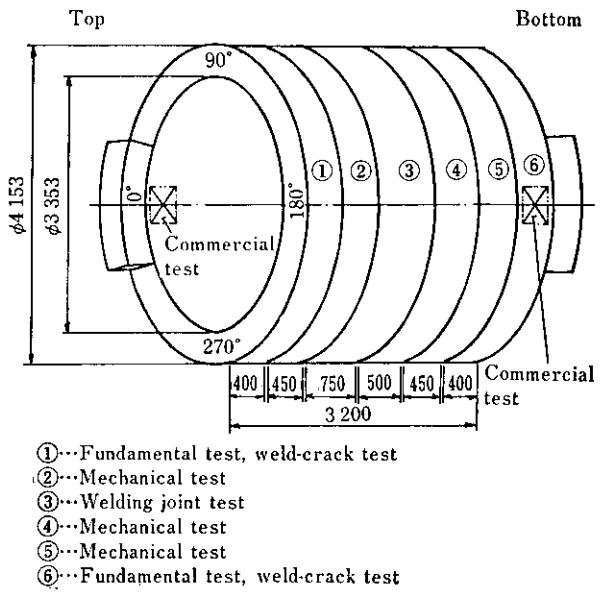

Fig. 6 Sampling position of test blocks

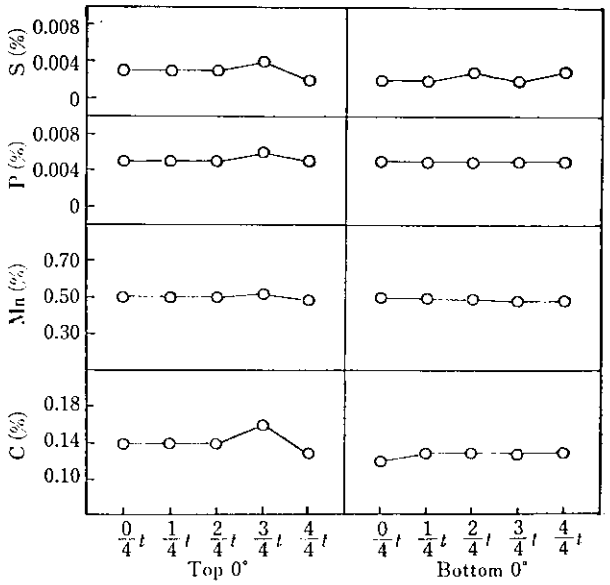

Fig. 7 Change of chemical composition at various positions through thickness

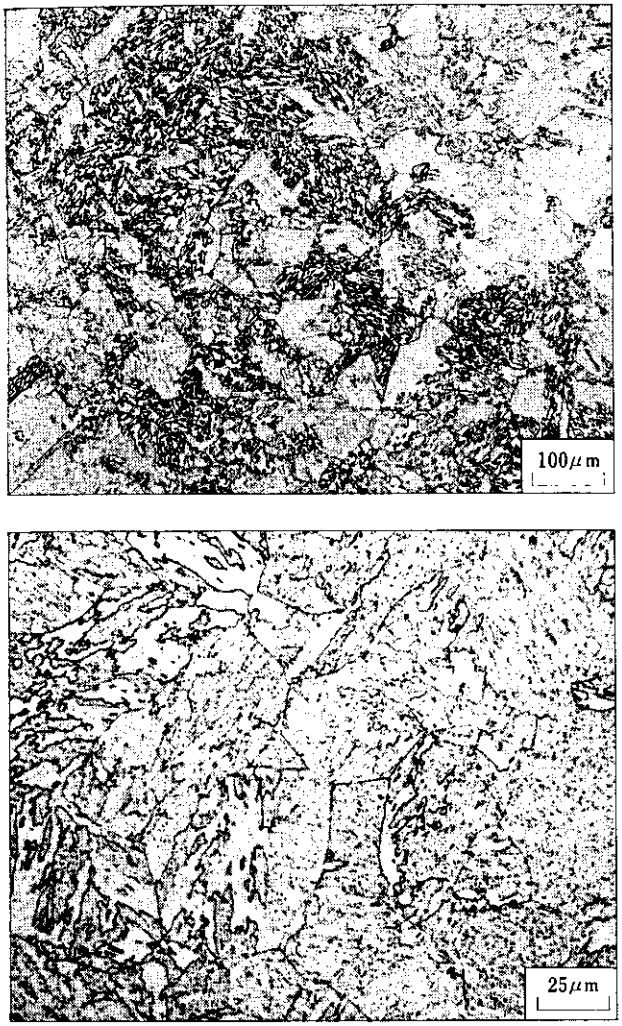

Photo 3 Typical microstructures of shell ring ($\frac{2}{4}t$)

3.3.2 Strength at room temperature and elevated temperatures

Figure 8 shows variations in tensile properties of the top and bottom. Strength values of both the top and the bottom are uniform in the whole section of the wall thickness of 400 mm. **Figure 9** shows the relationship between tensile properties and tempering parameter (T.P.). Strength decreases with increasing tempering parameter. The strength at room temperature specified in the ASME SA336 F22 is ensured when T.P. is 20.9×10^3 and less. The strength at elevated temperatures of $(\sigma_A) \times 4$ specified in the ASME Sec.

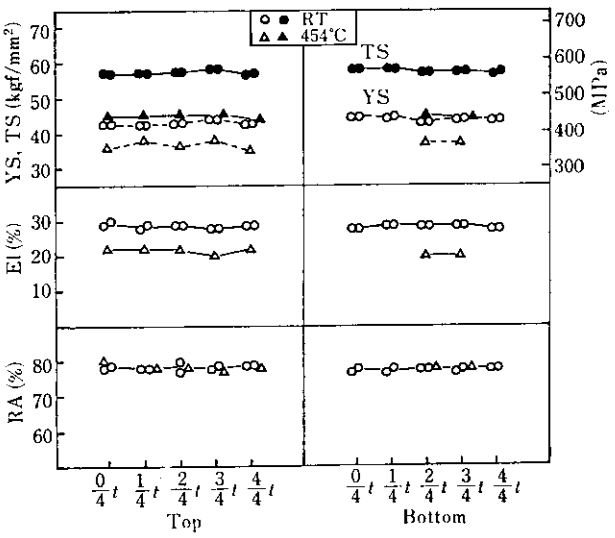

Fig. 8 Variation of tensile properties of tangential direction through thickness (PWHT: 690°C × 24.5 h)

Table 2 Cleanliness, d 60 × 400 by JIS G 0555, of shell ring

(%)

Sampling Position		dA (60×400)	dB (60×400)	dC (60×400)	dT (60×400)
Top	$\frac{0}{4}t$	0.029	0.000	0.000	0.029
	$\frac{1}{4}t$	0.037	0.000	0.000	0.037
	$\frac{2}{4}t$	0.033	0.000	0.000	0.033
	$\frac{3}{4}t$	0.033	0.000	0.000	0.033
	$\frac{4}{4}t$	0.033	0.000	0.000	0.033
Bottom	$\frac{0}{4}t$	0.037	0.000	0.000	0.037
	$\frac{1}{4}t$	0.025	0.000	0.000	0.025
	$\frac{2}{4}t$	0.033	0.000	0.000	0.033
	$\frac{3}{4}t$	0.033	0.000	0.000	0.033
	$\frac{4}{4}t$	0.037	0.000	0.000	0.037

Note Type A inclusion : Sulfide, Silicate
Type B inclusion : Alumina
Type C inclusion : Globular oxide

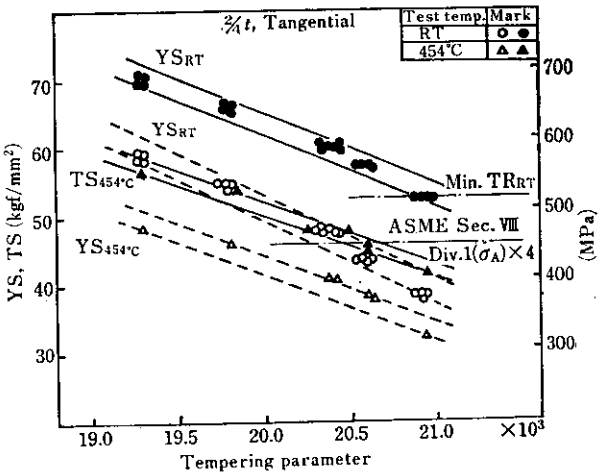

Fig. 9 Relation between tensile strength and tempering parameter

VIII Div. 1 is ensured when T.P. is 20.4×10^3 and less. Further, it is apparent from **Fig. 10** that the strength at elevated temperatures of 430 to 480°C can be obtained if strengths at room temperature of 60 kgf/mm² and over are ensured.

Figure 11 shows results of an investigation into creep strength. Since a low-Si steel was used, creep strength obtained shows values close to the upper limit of the conventional range. The difference in creep strength between the top and the bottom is small and the rupture stress of both the top and the bottom is as good as 80% and over.

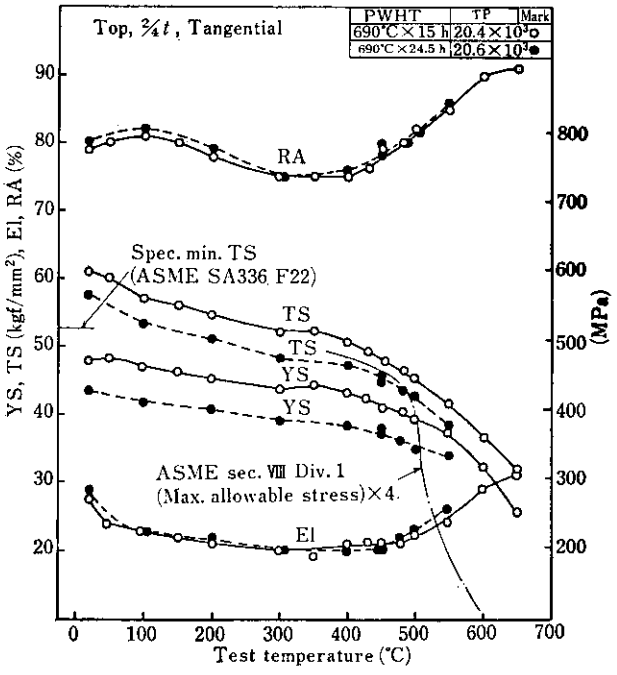

Fig. 10 Tensile properties at elevated temperature

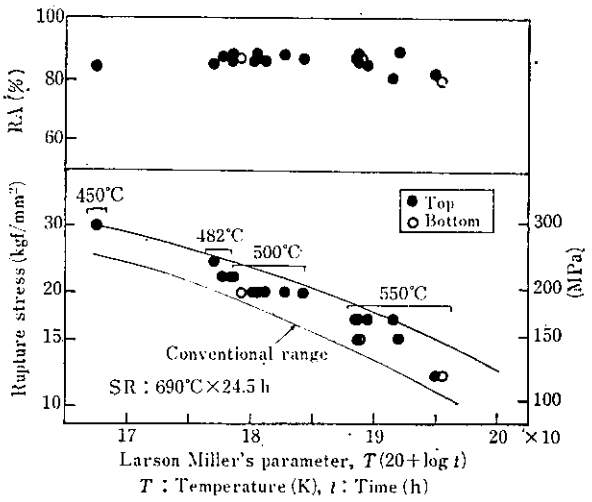

Fig. 11 Relation between rupture stress and Larson Miller's Parameter

3.3.3 Toughness and temper embrittlement susceptibility

Figure 12 shows variations in toughness of the top and the bottom. Although some dependence on the cooling rate is observed, ${}_vE_{-40}$ is 13 kgf·m and over and TT_{54J} after SC is −55°C and under even at the center. The difference in toughness between the top and the bottom is small and ΔTT_{54J} (difference in the transition temperature indicating 54J before and after SC) is also as small as 11°C and under. It may be said from these values that this hollow ingot is homogeneous and is little susceptible to temper embrittlement. This small temper embrittlement susceptibility is due greatly to the use of a basic oxygen furnace steel (for reduction in As, Sb and Sn) and the improvement in dephosphorizing techniques achieved by employing the double-blowing of the basic oxygen furance.

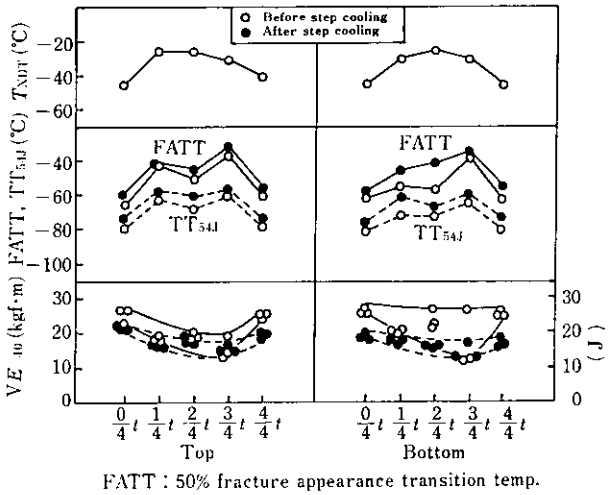

FATT : 50% fracture appearance transition temp.

Fig. 12 Variation of impact and drop weight properties of tangential direction through thickness (PWHT: 690°C × 24.5 h)

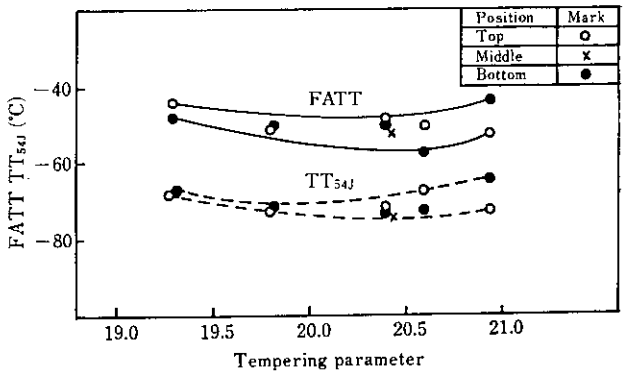

Fig. 13 Relation between transition temperature and tempering parameter ($\frac{2}{4}t$ tangential)

Figure 13 shows the relationship between toughness and tempering parameter. Toughness values are almost constant in the tempering parameter range of 19.3×10^3 to 20.9×10^3.

3.3.4 Fracture toughness

The three-point bending test, the CT test and the split pin and wedge type compact test were conducted on 25 mm thick, 25 mm thick and 50 mm thick specimens, respectively, to investigate fracture toughness values before and after SC. **Figures 14** to **16** show results of these tests.

The critical COD (δ) values shown in Fig. 14 were obtained from 25 mm thick specimens and do not always represent the critical COD of the tested material with an overall thickness of 400 mm. However,

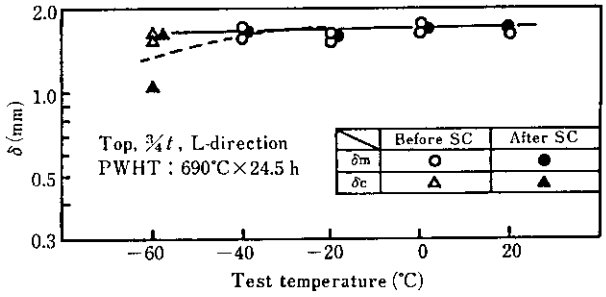

Fig. 14 COD values (δ) before and after step cooling at various temperature

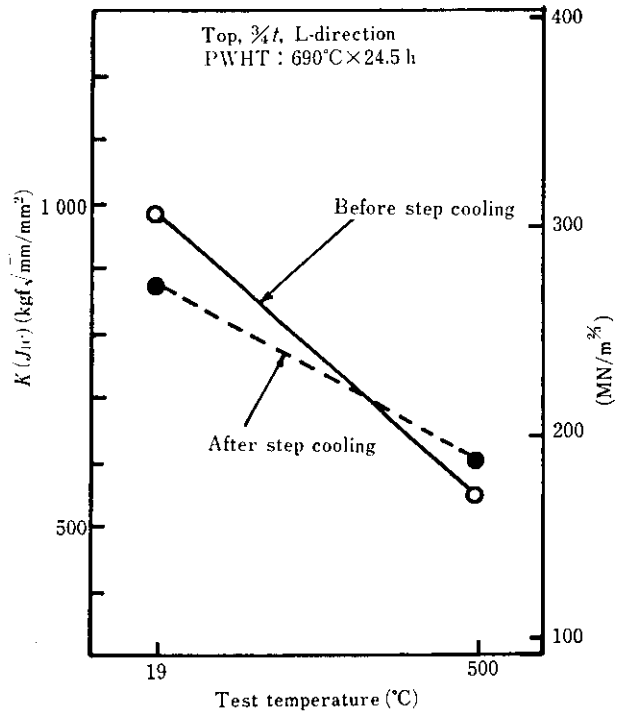

Fig. 15 $K(J_{Ic})$ values before and after step cooling at various temperatures

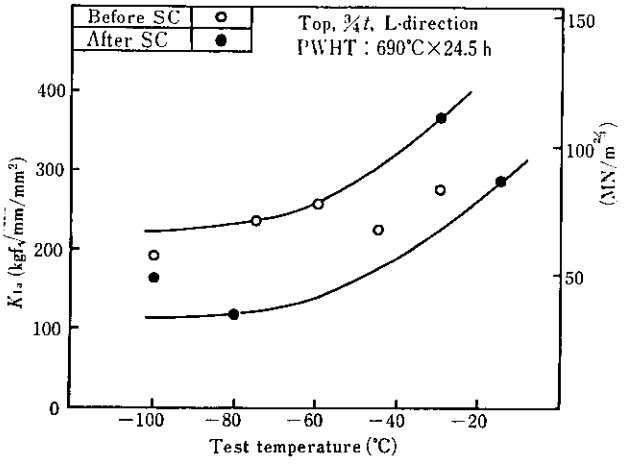

Fig. 16 Temperature dependence of K_{Ia} before and after step cooling

brittle fracture did not occur in the temperature range from room temperature to −40°C and the COD (δ_m) under the maximum load was obtained. This value was as good as approximately 1.6 mm. Though the maximum load came in under the range of brittle fracture at −60°C, the COD value was as large as 1 mm and over (refer to Fig. 14). All the COD-values obtained in this test are found in the upper shelf range. According to available data[4] on the dependence upon specimen thickness, the COD-value in the upper shelf range increases with inreasing specimen thickness. Therefore, it can be presumed that the COD for the overall thickness (400 mm) of the tested material at service temperatures (0°C and above) is larger than the value (approximately 1.6 mm) obtained in this experiment. The static fracture toughness (K_{Ic}) is represented as $K(J_{Ic})$ in Fig. 15. $K(J_{Ic})$-values before and after SC are approximately 900 kgf $\sqrt{\text{mm}}$/mm² at room temperature and approximately 600 kgf $\sqrt{\text{mm}}$/mm² at 500°C. These values are on a level with those of reactor pressure vessel steels[5].

The crack arrest toughness value (K_{Ia}) is 190 to 275 kgf $\sqrt{\text{mm}}$/mm² before SC and 120 to 365 kgf $\sqrt{\text{mm}}$/mm² after SC in the temperature range of −15 to −100°C, as shown in Fig. 16. Thus K_{Ia}-values are on a level with those[5] of reactor pressure vessel steels even after SC.

3.3.5 Fatigue properties

Figure 17 shows results of the low-cycle fatigue test at room temperature and an elevated temperature (482°C). The values at room temperature are almost in agreement with the ASME best fit curve and data[6] on 2¼Cr-1Mo steel plates and there is no difference between the manufacturing methods. Although the values at 482°C are on the short-life side compared

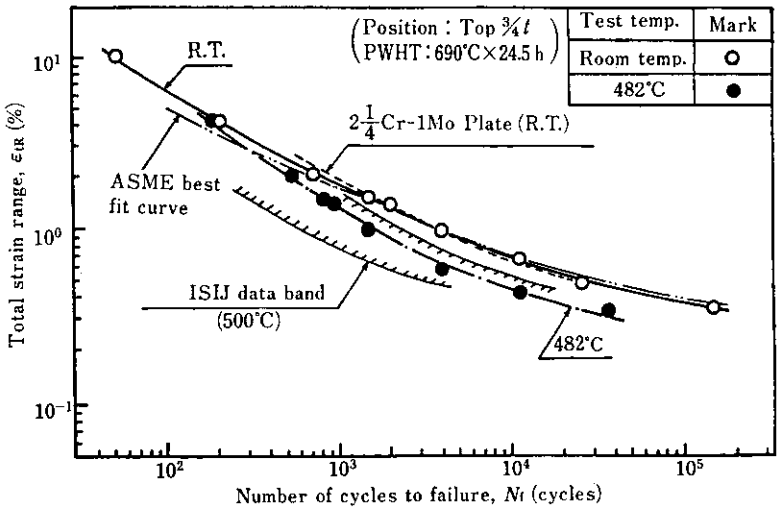

Fig. 17 Results of low cycle fatigue test of shell ring at room temperature and 482°C

with those obtained at room temperature, they are distributed on the upper part of the conventional data band[7]. Furthermore, the data at 482°C are in good agreement with results of estimation using a life estimation formula[8] in which damage due to oxidation is taken into consideration. Therefore, a decrease in life of this order caused by the temperature is judged to be reasonable.

3.3.6 Hydrogen attack

Specimens were taken from the positions of $\frac{0}{4}t$ (outermost part), $\frac{1}{4}t$, $\frac{2}{4}t$, $\frac{3}{4}t$ and $\frac{4}{4}t$ (innermost part) of the test blocks 1 and 6 in the thickness direction from the outer to the inner surface, and were immersed in an autoclave under a high-temperature high-pressure hydrogen atmosphere in order to conduct the hydrogen attack test. **Figure 18** shows results of the Charpy impact test at 0°C on specimens exposed at partial pressures of hydrogen, P_{H_2}, of 0 to 500 kgf/cm² and at a temperature of 500°C for an exposure time of 100 h. A decrease in absorbed energy by exposure is not observed in the top or the bottom, nor is there any differences. **Figure 19** shows results of the Charpy impact test at 0°C on specimens treated at P_{H_2} of 500 kgf/cm² and at a temperature of 500°C for various exposure times. Figures 18 and 19 reveal that the deterioration

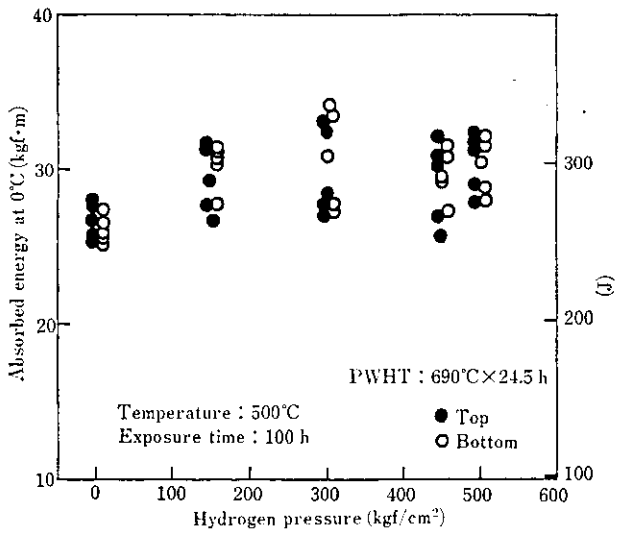

Fig. 18 Effect of hydrogen pressure on absorbed energy at 0°C

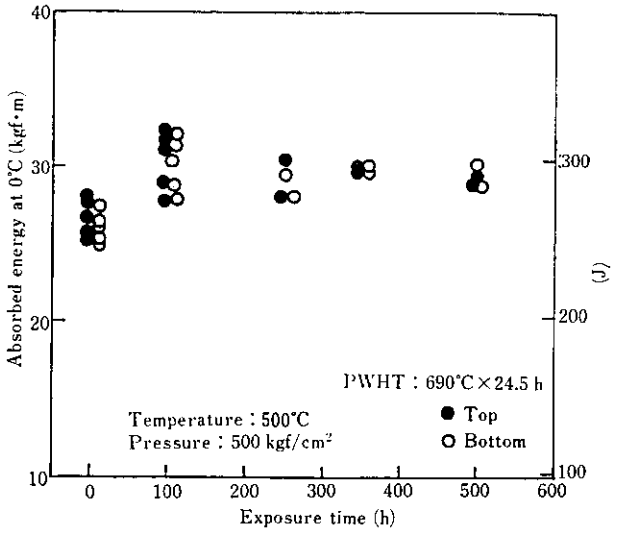

Fig. 19 Effect of exposure time on absorbed energy at 0°C

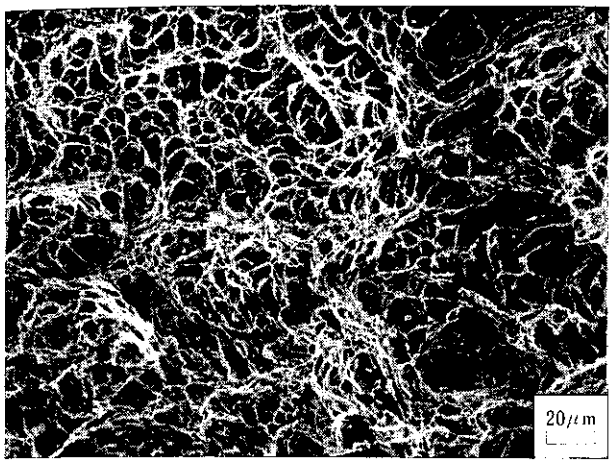

Hydrogen pressure : 500 kgf/cm², Temp. : 500°C
Exposure time : 500 h

Photo 4 Fractured surface at 0°C shown in test steel exposed in hydrogen circumstance

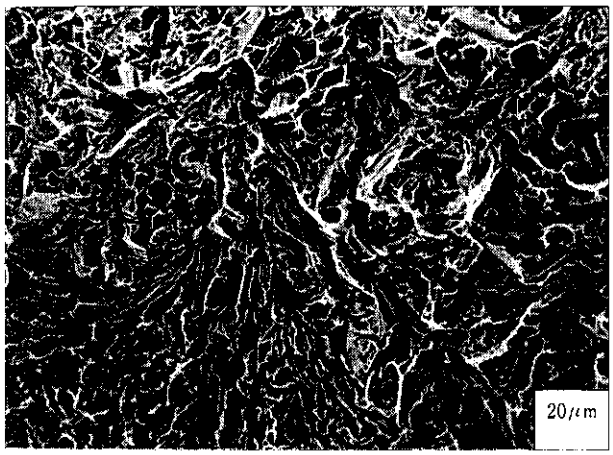

(a) Non-treated steel (As Q. T.)

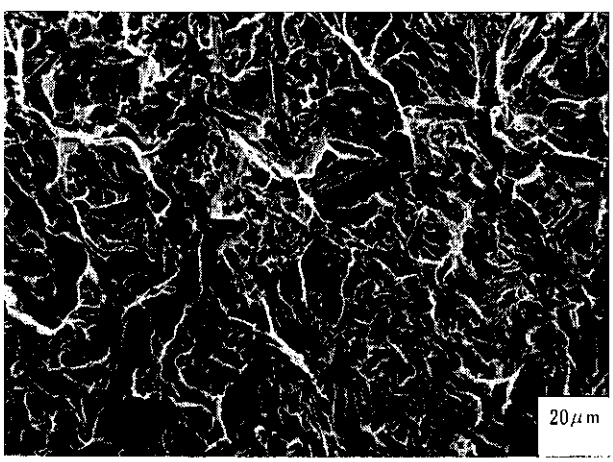

(b) Hydrogen attacked steel
(500 kgf/cm², 500°C, 500h)

Photo 5 Fractured surface of two types of steel at liquid N_2 temperature

by hydrogen attack is not observed under the experimental conditions. **Photo 4** shows a scanning electron micrograph of a fractured surface after the Charpy impact test at 0°C conducted on a specimen exposed at a partial pressure of hydrogen of 500 kgf/cm² and at a temperature of 500°C for an exposure time of 500 h. Dimple patterns are observed on the whole fractured surface. **Photo 5** (a) shows a scanning electron micrograph of a fractured surface when a specimen in the as-tempered condition (T.P. = 20.6×10^3) was broken at the liquid nitrogen temperature. **Photo 5** (b) shows a scanning electron micrograph of the fractured surface of a specimen similarly fractured after exposure. The two fractured surfaces show cleavage fracture. This means that integranular embrittlement by hydrogen attack did not occur in the tested material under the conditions of this experiment.

4 Discussion

4.1 Homogeneity of Hollow Ingots

As is apparent from the reports[9,10], the homogeneity of hollow ingots has been confirmed. As shown in Fig. 7, the results of a chemical composition analysis of the product reveal that the hollow ingot used is homogeneous. These results are almost the same as

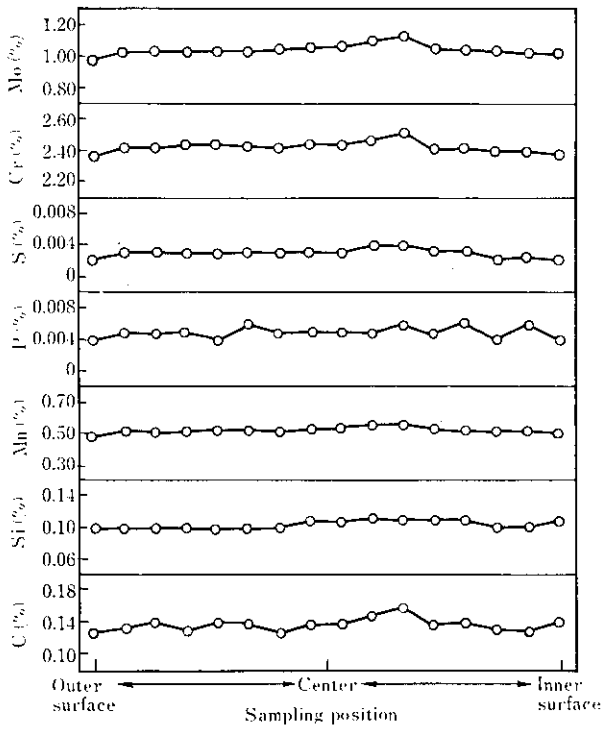

Fig. 20 Segregation of chemical elements near hot top of 200 t hollow ingot

those of reactor vessel steel products produced from hollow ingots. Furthermore, the chemical composition of the part of the ingot near the hot top was analyzed to confirm the homogeneity of the whole ingot. As is evident from the results of this investigation shown in **Fig. 20**, almost the same tendency as in previous investgations is observed; that is to say, the segregation of each component is slight even in the area just under the hot top and this area is very homogeneous. This suggests that the crop to be cut at the top of the ingot is small. This homogeneity results in good mechanical properties and is considered to have a good effect on internal build-up welding, which has already been confirmed.

4.2 Hydrogen Attack

Hydrogen attack is a phenomenon in which carbide precipitates in steel and the hydrogen that has infiltrated into steel at a high temperature and under a high pressure react with each other with the evolution of methane gas bubbles, reducing the ductility and toughness of steel products. Therefore, the physical and chemical properties of carbides in steel influence steel's resistance to hydrogen attack.

An investigation was made into carbide precipitates in tempered specimens of a low-Si (0.05%) steel and a high-Si (0.6%) steel. **Photo 6** shows electron micrographs of these precipitates by the carbon extraction replica method and composition mapping by EDX (energy dispersive X-ray spectroscopy)[11-13]. The X-ray intensity ratio of Cr and Fe in precipitates varies depending on the Si content. That is to say, it is apparent that Fe intensity is high at a high Si content, whereas Cr intensity is high at a low Si content. From results of electron microscopy, it is made clear that the proportion of Fe in carbides increases with increasing Si content and that the transition from the M_7C_3 type to the $M_{23}C_6$ type takes place at the same time[11,16]. The stability of carbide precipitates is weakened by the Si contained; as a result, carbide precipitates of high Si content are apt to be decomposed by hydrogen atoms that have infiltrated into steel under a high-temperature high-pressure hydrogen atmosphere, and are susceptible to hydrogen attack.

The incubation period, t_i(h), until the start of deterioration in the mechanical properties caused by hydrogen attack is generally given by the following equation[14]:

$$t_i = CP_{H_2}^{-n} \exp(Q/RT)$$

P_{H_2}: Partial pressure of hydrogen (kgf/cm²)
T: Temperature (K)
R: Gas constant
Q: Apparent activation energy for the incubation period (cal/mol)
C: Constant

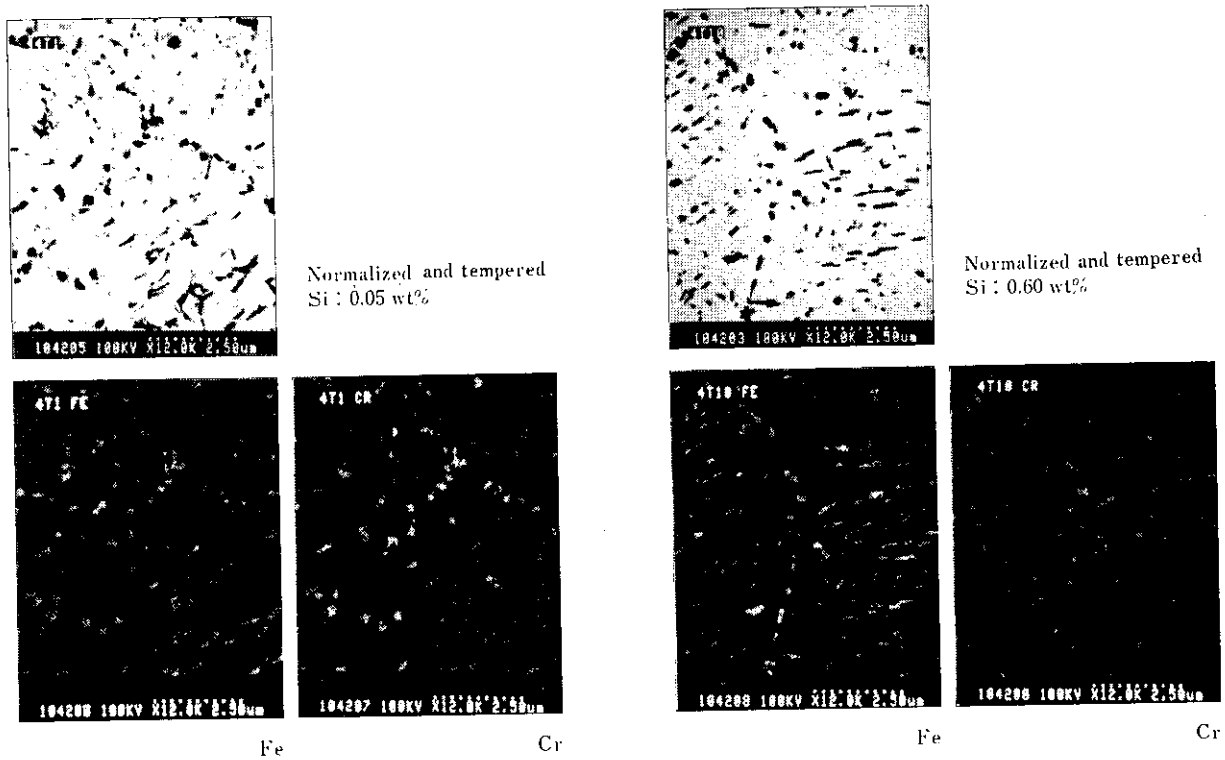

Photo 6 X-ray mapping of carbides in 2¼Cr-1Mo steels showing the effect of Si on carbide composition

According to results of an investigation into the effect of Si on hydrogen attack by the authors[12,15], $n \cong 3$ and $Q \cong 32\,000$ cal/mol. When C is calculated using these values and the condition of $t > 500$ h obtained under the exposure conditions of $P_{H_2} = 500$ kgf/cm² and $T = 500$°C, the value of C over 60 is obtained. When a case where the material used in this experiment is used under the conditions of $P_{H_2} = 150$ kgf/cm² and $T = 455$°C is examined, then $t_t > 100\,000$ h. Thus hydrogen attack does not occur until more than 10 years elapse. Incidentally, t_t is less than 10 years when the Si content is approximately 0.30% as usual. The foregoing suggests that it is important to reduce the Si content of base metal as a basic concept of alloy designing aimed at anti-hydrogen attack. The hollow ingot used in this experiment was made based on this basic concept, and may be said to be excellent in anti-hydrogen attack properties, as shown in Figs. 18 and 19.

5 Conclusions

A 400 mm thick shell ring of 2¼Cr-1Mo steel of low-Si and low-P content was produced by forging a 200 t hollow ingot made by the BOF-RH process. High-temperature hardening was performed to give hardenability to this heavy-wall material. The adoption of the BOF-RH process for the manufacture of the hollow ingot is advantageous in terms of reduction of impurity elements, cleanliness and homogeneity. This process is best suited for the production of steels under a high-temperature high-pressure hydrogen atmosphere. It has been made clear that low Si and P contents are generally effective in improving temper embrittlement susceptibility, anti-hydrogen attack properties and creep strength. Furthermore, it has become apparent that the high-temperature hardening technique developed by Kawasaki Steel is capable of providing high strength and high toughness for extra-heavy-wall products.

The authors are confident that the accumulation of these comprehensive data will lead to a stable manufacture of steels for oil refinery pressure vessels, thereby sufficiently meeting the growing demand of pressure vessel manufacturers.

References

1) Y. Kusuhara, T. Sekine, T. Enami, H. Ooi: "BOF-LRF Refined Ultra-low Phosphorus 2.25Cr-1MO Steel Plate of Low Temper Embrittliment Susceptibility", 4th International Conference on Pressure Vessel Technology
2) S. Sato, Y. Ono: *Kawasaki Steel Technical Report*, **12** (1980) 1, p. 115 (in Japanese)
3) M. Takada, H. Wanaka, K. Aso, Y. Arakawa et al.: *Kawasaki Steel Giho*, **14** (1982) 4, p. 424
4) Japan Welding Engineering Society, Steel Sectional Meeting, FTC Committee: "A Study on Fracture Toughness Criterion" (Feb., 1981)
5) Y. Nakano, K. Sano, M. Tanaka, N. Ohashi: *Kawasaki Steel Giho*, **12** (1980) 4, p. 33
6) A. Narumoto et al.: *Kawasaki Steel Technical Report*, **12** (1980) 1, p. 207 (in Japanese)
7) Iron and Steel Institute of Japan, Creep Committee, Subcommittee on Thermal Fatigue Testing at Elevated Temperature: "Cooperative Research Report on Thermal Fatigue Properties at Elevated Temperature of 2¼Cr-1Mo Steel", (June, 1978)
8) A. Narumoto, M. Tanaka, A. Kamata: *Tetsu-to-Hagané*, **67** (1981) 9, A208
9) Y. Iida, T. Yamamoto, S. Yamaura, K. Aso, J. Matsuno, T. Nishioka: *Tetsu-to-Hagané*, **66** (1980) 2, p. 211
10) Y. Iida, H. Wanaka, T. Yamamoto, K. Aso, J. Matsuno: "Development of Hollow Steel Ingot for Large Forging", *World Steel & Metalworking*, (1982) 4, p. 218
11) T. Imanaka, J. Shimomura: Japan Petroleum Institute, Facilities Sectional Committee, Symposium, (Dec., 1982)
12) T. Imanaka: *Bulletin of the Japan Institute of Metals, Symposium*, (Sept., 1982), No. 125
13) T. Imanaka, J. Shimomura: *Bulletin of the Japan Institute of Metals*, (Apr., 1983), No. 160
14) L.C. Weiner: *Corrosion*, **17** (1961), p. 137
15) T. Imanaka and J. Shimomura: To be published in 5th International Conference on Pressure Vessel Technology
16) G.H. Geiger and O.F. Angeles: API Pub., (1975) 945, p.9